Evidence of an enhanced nuclear radius of the α-halo state via $\alpha + {}^{12}$C inelastic scattering

Makoto Ito

Department of Pure and Applied Physics, Kansai University, Yamatecho, 3-3-35, Suita, Japan, and Research Center for Nuclear Physics (RCNP), Osaka University, Mihogaoka 10-1, Suita 567-0047, Japan

(Received 25 August 2016; revised manuscript received 10 February 2018; published 17 April 2018)

Evidence of the enhanced nuclear radius in the Hoyle rotational state, 2_2^+, is derived from the differential cross sections in $\alpha + {}^{12}$C inelastic scattering. The prominent shrinkage is observed in the differential cross section of the 2_2^+ state in comparison to the yrast 2_1^+ state, and this shrinkage is the first evidence of the enhanced nuclear radius which originates from the 3α structure in the 2_2^+ state. A diffraction formula, that is, Blair's phase rule, is applied to the differential cross sections, and the present analysis predicts an enhancement of 0.6 to 1.0 fm in the nuclear radius of the 2_2^+ state in comparison to the radius of the yrast 2_1^+, which is considered to have a normal nuclear radius. Constraint on the recent *ab initio* calculation for 3α states in ^{12}C is also discussed.

DOI: 10.1103/PhysRevC.97.044608

I. INTRODUCTION

Nuclei in nature are composed of almost the same number of neutrons (N) and protons (Z). In the ground state of a nucleus, neutrons and protons are tightly bound and perform independent particle motion in a self-consistent mean field. The nuclear radius is proportional to $A^{1/3}$, where A is the mass number of the nucleus, due to the saturation property of the nuclear density [1]. Thus, the nuclear radius smoothly varies as a function of A. Recently, so-called neutron-excess nuclei ($N > Z$) have been artificially synthesized, and enhancements of the nuclear radius from the empirical formula $\propto A^{1/3}$ confirmed [2]. This enhanced radius is called the neutron halo (or skin) phenomenon, in which extra neutrons largely penetrate the classical turning point due to the quantum tunneling effect. A typical example of a neutron halo can be seen in ^{11}Li, which has the three-body structure of a ^{9}Li core plus two neutrons. The nuclear radius of ^{11}Li is enhanced by about 1 fm in comparison to the usual $\propto A^{1/3}$ rule [2].

On the contrary, cluster structures, in which a nucleus is decomposed into several subunits, are realized in the low excited states of light-mass nuclei [3]. In the cluster structure, the subunits are weakly coupled to each other, and their nuclear radius is prominently extended in comparison to the radius of the ground state, which obeys the law of $\propto A^{1/3}$. In particular, this enhancement of the nuclear radius is extensive in the 3α structure of the ^{12}C nucleus [4,5]. The ground state of ^{12}C has a radius of 2.40 fm [4] with a spin parity of 0^+ (0_1^+), while the excited 0_2^+ state at $E_x = 7.65$ MeV, which is called the Hoyle state, is considered to have a radius of 3.47 fm with a well-developed 3α cluster structure [4]. The extension of the radius in 0_2^+ is predicted to be about 1 fm, which is comparable to the extension of neutron halos. In this article, I propose a new method to obtain a signature of the enhanced nuclear radius of the 3α cluster state.

Unfortunately, direct measurement of the radius of Hoyle 0_2^+ states with a developed 3α cluster structure is impossible due to its short lifetime, but there have been several attempts to obtain evidence of an enhanced nuclear radius of 3α Hoyle states from inelastic scattering of ^{12}C, which excites the Hoyle 0_2^+ state as a final state. In the inelastic scattering of light ions by ^{12}C, an oscillating pattern in the differential cross section of the scattered ion is discussed in connection to the enhanced radius of the final 0_2^+ state with a 3α structure [6–8].

In the proton scattering at $E_p = 1040$ MeV, the diffraction radius was derived from the differential cross section for the inelastic scattering of $^{12}\mathrm{C}_{\mathrm{g.s.}} \rightarrow {}^{12}\mathrm{C}(0_2^+)$ according to the extended formula of Blair's phase rule [7]. The application of this formula to the cross section gives the enhanced diffraction radius for this final channel in comparison to the elastic ^{12}C(0_1^+) channel and the inelastic channel going to ^{12}C(2_1^+). On the other hand, in the α scattering at $E_\alpha = 240$ MeV, the evolution of the Airy minimum was pointed out in the final channel of ^{12}C(0_2^+) [8]. The number of Airy minima in the ^{12}C(0_2^+) channel seems to be increased in comparison to that in the other noncluster channels, such as the ^{12}C(0_1^+, 2_1^+, 3_1^-) channels. These anomalous behaviors identified in the differential cross sections are discussed in connection to the enhanced nuclear radius of the Hoyle 0_2^+ state [7,8].

However, subsequent analyses demonstrated that the oscillation pattern in the cross section, such as a peak or valley position in the angular distribution, is not very sensitive to the nuclear radius of the final 0_2^+ state [9,10]. In Ref. [9], the sensitivity of the inelastic differential cross sections going to the 0_2^+ channel is checked by varying the nuclear radius of the final 0_2^+ state, and the peak and minimum positions are not very sensitive to the variation of the final radius. According to the analysis, the author concluded that the differential cross section is mainly determined by the spatial size of the coupling potential, which induces the transition ^{12}C(0_1^+) $\rightarrow$ ^{12}C(0_2^+). Therefore, the relation of the extended radius in the ^{12}C(0_2^+) state, which is generated as the final channel in inelastic scattering, and the oscillation pattern in the cross section for the final ^{12}C(0_1^+) channel remains unclear.

As demonstrated in Ref. [9], the sensitivity of the cross section to the variation of the nuclear radius of the final 0_2^+ state is not very strong but the inelastic scattering, which is induced by the coupling potential, is expected to contain the size information on the final 0_2^+ state because the coupling potential contains considerable size information on the final-state wave function. However, I consider that extraction of evidence of an enhanced size of the Hoyle 0_2^+ state from inelastic scattering is difficult. This is because there is no appropriate "reference (inelastic) 0^+ channel" to be compared with the Hoyle 0_2^+ channel. One might consider that the enhancement factor of the 0_2^+ state can be obtained from comparison with the elastic 0_1^+ channel but this comparison is completely meaningless because the 0_1^+ channel corresponds to elastic scattering, which is a completely different process from inelastic scattering, going to the 0_2^+ channel. Furthermore, comparison of the 0_2^+ channels with the other noncluster channels, such as the 2_1^+ and 3_1^- channels, is inappropriate because the latter noncluster channels have a finite spin, which strongly affects the oscillation pattern in the differential cross section.

In previous studies of inelastic scattering and the nuclear radius of the 0_2^+ state, the most crucial problem is difficulty setting the reference channel, which should be appropriately compared with 0_2^+. In a comparison of the 0_2^+ channel with the other noncluster channels, 0_1^+, 2_1^+, and 3_1^-, which is discussed in the pioneering works [7,8], it is difficult to find the enhancement factor for a 0_2^+ state with a large radius. Therefore, one must introduce a new viewpoint into the discussion of inelastic scattering as a tool to derive an enhanced nuclear radius in 3α cluster states. In this article, I focus on the 2_2^+ state, which corresponds to the 3α rotational state of the Hoyle 0_2^+ state [4,5] with a life of 10^{-21} s (width of $\Gamma \approx 1$ MeV), and demonstrate that direct evidence of an enhanced nuclear radius in the 2_2^+ state clearly appears in $\alpha + {}^{12}\mathrm{C}$ inelastic scattering. In a modern theory, the Hoyle rotational 2_2^+ state, which was recently identified in experiments [11], is interpreted in terms of an α-halo state with a dilute 3α structure [5].

In the present analysis, the differential cross section $\alpha + {}^{12}\mathrm{C}(0_1^+) \to \alpha + {}^{12}\mathrm{C}(2_2^+)$ is compared with the reference reaction $\alpha + {}^{12}\mathrm{C}(0_1^+) \to \alpha + {}^{12}\mathrm{C}(2_1^+)$, in which the 2_1^+ state is a rotational state of the ground 0_1^+ state with a spatially compact structure. In the inelastic scattering to the $2_{1,2}^+$ states, the kinematic conditions are almost the same but only the radii are prominently different, say 2.4 fm for 2_1^+ and 4.0 fm for 2_2^+ [4]. Thus, the enhanced radius in the 2_2^+ state can be clearly discussed on the basis of the "reference channel," that is, the 2_1^+ channel. The comparison of these two inelastic scatterings is expected to provide direct evidence of an extended nuclear radius of the 2_2^+ state, which involves the 3α cluster structure.

The organization of this article is as follows: In Sec. II, the theoretical framework of microscopic coupled channels (MCC) is explained. Application of the MCC calculation to the $\alpha + {}^{12}\mathrm{C}$ inelastic scattering at $E_\alpha = 386$ MeV, which has recently been observed, is shown in Sec. III. From the theoretical calculation, direct evidence of the enhanced nuclear radius in the 2_2^+ state is demonstrated. The final section (IV) is devoted to a summary and discussion.

II. FRAMEWORK

I calculate the differential cross sections of an α particle scattered by ${}^{12}\mathrm{C}$ in the formulation of the microscopic coupled-channels calculation [8,12]. In the MCC calculation, the nuclear potential of α and ${}^{12}\mathrm{C}$ is calculated from the double-folding model, which is symbolically written as a function of the α-${}^{12}\mathrm{C}$ relative coordinate of $\mathbf{R}$,

$$V_{f,i}(\mathbf{R}) = \iint \rho_{f,i}^{({}^{12}C)}(\mathbf{r}_1)\rho^{(\alpha)}(\mathbf{r}_2)v_{\mathrm{NN}}(\mathbf{s})d\mathbf{r}_1 d\mathbf{r}_2, \quad (1)$$

with $\mathbf{s} = \mathbf{r}_2 - \mathbf{r}_1 - \mathbf{R}$. Here $\mathbf{r}_1$ ($\mathbf{r}_2$) denotes a coordinate measured from the center of mass (c.m.) in the ${}^{12}\mathrm{C}$ (α) nucleus. $\rho_{f,i}(\mathbf{r})$ represents the diagonal ($f = i$) or transition ($f \neq i$) density of ${}^{12}\mathrm{C}$, which is calculated by the microscopic 3α cluster model, resonating group method [4], while $\rho^{(\alpha)}(\mathbf{r})$ denotes the density of the α particle, which reproduces the charge form factor of the electron scattering. In Eq. (1), v_{NN} represents the effective nucleon-nucleon (NN) interaction, which acts between a pair of nucleons contained in the ${}^{12}\mathrm{C}$ nucleus and the α particle. In the present calculation, I adopt the DDM3Y (density-dependent Michigan 3-range Yukawa) interaction [13].

In addition to the folding potential, I introduce the absorptive potential ($-iW$) with the Saxon-Woods form factor in the diagonal ($f = i$) transition in order to simulate other reaction processes [8], and the parameter set of Saxon-Woods is tuned so as to reproduce all of the observed differential cross sections as much as possible. The three parameters in the absorptive Saxon-Woods potential for the individual channels, that is, the diffuseness a, the radius R, and the strength W, are listed in the Appendix. The final expression of the coupling potential, $U_{f,i}$, for the transition of $i \to f$ becomes

$$U_{f,i}(\mathbf{R}) = N_{\mathrm{R}} \cdot V_{f,i}(\mathbf{R}) + V_C(R) \cdot \delta_{f,i} - iW(R) \cdot \delta_{f,i}, \quad (2)$$

where V_C denotes the Coulomb potential, which is calculated by assuming a uniformly charged sphere. In the present MCC calculation, I neglect the Coulomb excitation because of the lighter-mass system. In Eq. (2), the normalization factor N_R is introduced into the double-folding potential because the folding potential contains a theoretical ambiguity in its strength. Here this factor is set to $N_R = 1.30$, which is consistent with the MCC calculation in Ref. [8].

As for the internal excitation of ${}^{12}\mathrm{C}$, I include the discrete states around the breakup threshold of ${}^{12}\mathrm{C} \to 3\alpha$ at $E_{\mathrm{th}} = 7.27$ MeV in addition to the ground 0_1^+ state: the rotational 2_1^+ ($E_x = 4.44$ MeV), the vibrational 3_1^- (9.64 MeV), and the 3α cluster states, that is, 0_2^+ (7.65 MeV), 0_3^+ (14.04 MeV), and 2_2^+ (10.30 MeV).

III. RESULTS

I have solved the coupled-channels equation for the $\alpha + {}^{12}\mathrm{C}$ scattering at $E_\alpha = 386$ MeV [11] with the nuclear interaction in Eqs. (1) and (2). In Fig. 1, the calculated cross sections (solid curves) are compared with the experimental data (filled circles). The MCC calculation nicely reproduces the differential cross sections of the scattering to discrete bound or resonant

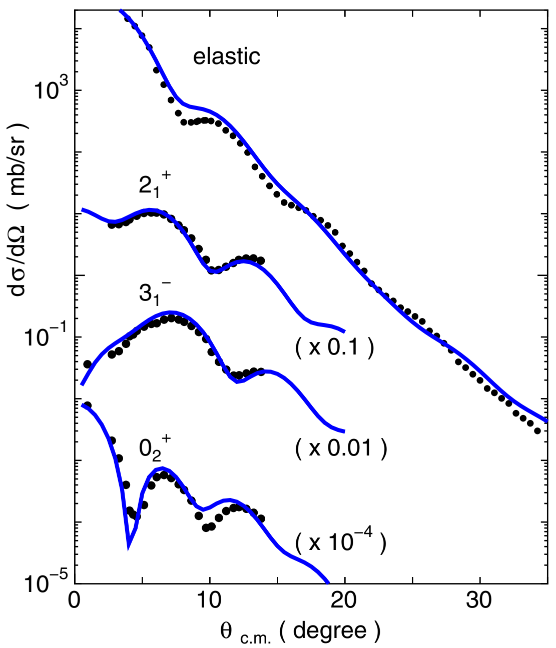

FIG. 1. Comparison of the MCC calculation with the observed differential cross section in $\alpha + {}^{12}\mathrm{C}$ scattering at $E_\alpha =$ 386 MeV [11]. Filled curves represent theoretical calculations; filled circles, experimental data. From top to bottom, results represent the elastic, 2_1^+, 3_1^-, and 0_2^+ channels, respectively.

states in ${}^{12}\mathrm{C}$, that is, from top to bottom, the elastic 0_1^+, 2_1^+, 3_1^-, and 0_2^+ channels. In particular, the 2_1^+ channel, which is the reference channel in discussing the enhanced nuclear radius of the 2_2^+ state, is nicely reproduced over the whole angular range.

In Fig. 2, the MCC calculation is compared with the differential cross section of the final excited state at $E_x \approx 10$ MeV, which is considered to be an incoherent mixture of the 0_3^+ and 2_2^+ channels, which have well-developed 3α cluster structures. The theoretical calculation (thick solid curve), which is constructed by incoherent summation of the 0_3^+ (dotted curve) and 2_2^+ (thin solid curve) channels, nicely reproduces the cross section of the excited state at $E_x \approx 10$ MeV in experiment (open circles). In this calculation, I have checked several parameter sets for the absorptive potential and artificially varied the mixing weight of these two channels. However, an incoherent mixture of these two contributions with almost the same weight is essential to reproduce the observed distribution, especially the structure of the smeared valleys in the angular distribution around $\theta_{\mathrm{c.m.}} \approx 5^\circ$ and 10°.

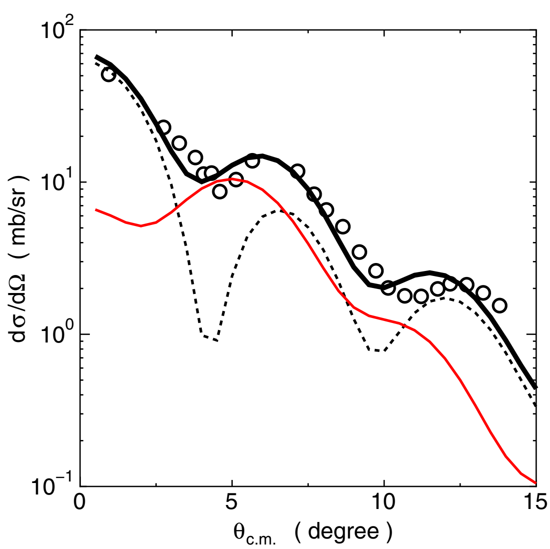

FIG. 2. Comparison of the theoretical calculation with the observed cross section of the excited state at $E_x \approx 10$ MeV. Open circles show experimental data, while the thick solid curve represents the total cross section in theory, which is given by the incoherent summation of the 0_3^+ (dotted curve) and 2_2^+ (thin solid curve) channels.

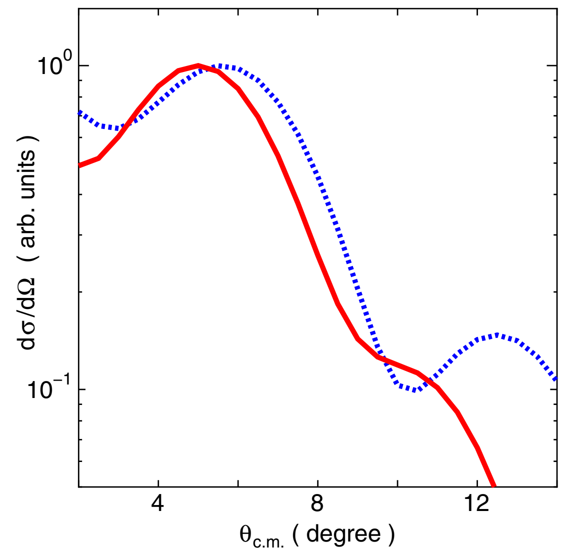

FIG. 3. Theoretical differential cross sections of the final 2_1^+ (dotted curve) and 2_2^+ (solid curve) channels in $\alpha + {}^{12}\mathrm{C}$ inelastic scattering. The former and latter cross sections are same as the cross sections shown in Figs. 1 and 2, respectively. The magnitudes of both cross sections are normalized by the maximum value around $\theta_{\mathrm{c.m.}} \approx 5^\circ$.

A comparison of the 2_1^+ cross section in Fig. 1 with the 2_2^+ in Fig. 2 is presented in Fig. 3. The peak position of the 2_2^+ cross section (solid curve) shifts to the forward angular region, and its angular distribution shows shrinkage and a rapid fall-down structure in comparison to the 2_1^+ cross section (dotted curve). The shift and shrinkage features are completely consistent with the result of multipole decomposition analysis of the experimental cross section, which is performed in the range $\theta_{\mathrm{c.m.}} < 15^\circ$ [11].

The shrinkage in the 2_2^+ cross section (solid curve in Fig. 3) is the first evidence of an extended size of the final 2_2^+ states, which can be confirmed by a direct observable, the differential cross section. Inelastic scattering to the 2_1^+ and 2_2^+ channels is the same regarding the reaction kinematics except for the excitation energy, and the size of the final state is different: a spatially compact structure in 2_1^+ with almost the same radius as the ground 0_1^+ state and a developed 3α structure in 2_2^+ having an extended radius. Thus, I conclude that the shrinkage in the 2_2^+ cross section originates from the spatially extended structure of the Hoyle rotational 2_2^+ state if the difference in

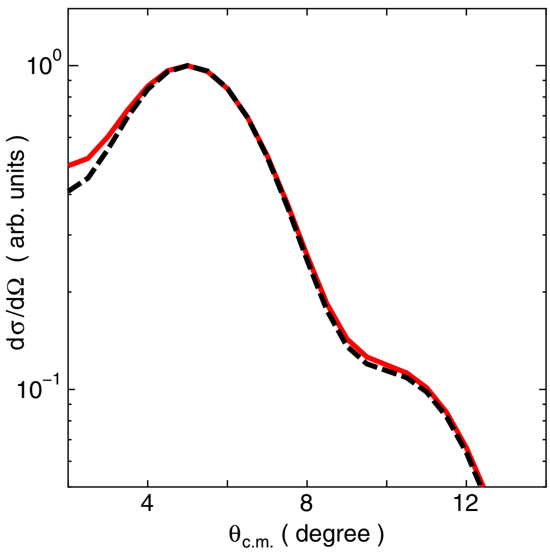

FIG. 4. Theoretical differential cross sections of the final channels of 2_2^+ with excitation energy $E_x = 10.3$ MeV (solid curve) and $E_x = 4.44$ MeV (dashed curve). The former cross section is the same as the cross sections shown in Fig. 2 (thin solid curve) and Fig. 3 (solid curve). The magnitudes of both cross sections are normalized by the maximum value around $\theta_{\mathrm{c.m.}} \approx 5^\circ$.

the excitation energies, that is, $E_x = 4.44$ MeV for 2_1^+ and $E_x = 10.3$ MeV for 2_2^+, can be safely neglected.

Not only the nuclear radius of the final state but also its excitation energy generally affects the oscillation pattern in the differential cross section. The relation of the excitation energy and the differential cross section has been investigated in our previous work on monopole excitation in $p + {}^{12}\mathrm{C}$ scattering [14]. If the excitation energy is low, the angular range of the differential cross section tends to shrink because a scattered particle can carry a high kinetic energy, which enhances the intensity of the forward scattering [14]. In order to examine the effect of the excitation energy more deeply, I artificially change the excitation energy of 2_2^+ (10.3 MeV) to that of 2_1^+ (4.44 MeV) by keeping the potential parameters unchanged, and the MCC calculation is reperformed.

In Fig. 4, the differential cross section of the "virtual 2_2^+ channel ($E_x = 4.44$ MeV)" is compared to that of the "realistic 2_2^+ channel ($E_x = 10.3$ MeV)." In this calculation, the angular distribution of the 2_1^+ channel, which is shown in Figs. 1 and 3, is almost unchanged. In Fig. 4, the angular distribution of the virtual 2_2^+ channel (dashed curve) is shrunk little in comparison to the distribution of the realistic 2_2^+ channel (solid curve). This shrinkage in the virtual state with the lower excitation energy is consistent with the result of monopole excitation [14]. The result in Fig. 4 means that the 2_2^+ cross section shrinks more if the excitation energy of 2_2^+ is exactly the same as that of 2_1^+. Since the excitation energy of the 2_2^+ state is higher than the energy of the 2_1^+ state in the realistic situation, the shrinkage of the 2_2^+ distribution shown in Fig. 3 is clear evidence of an enhanced radius of the 2_2^+ state, which overcomes the effect of the high excitation energy of this state.

I try to convert the differential cross sections in Fig. 3 into the spatial size for final-state production. If a nucleus is regarded as a "black sphere," which corresponds to a completely absorptive object, the radius of the black sphere can be determined by applying the theory of Fraunhofer diffraction to the differential cross section of the inelastic scattering. According to Blair's formula in Refs. [8] and [16], the oscillation pattern of the differential cross section for $0^+ \to 2^+$ inelastic scattering can be parametrized by a Bessel function of rank m, $J_m(x)$,

$$\frac{d\sigma}{d\Omega}(0^+ \to 2^+) \propto J_0(x)^2 + 3J_2(x)^2, \tag{3}$$

with the definition of $x = 2ka \sin(\theta_{\mathrm{c.m.}}/2)$. Here, k is the incident momentum, and a is the radius of the black sphere for diffraction scattering [7,15,16]. The black-sphere radius a can be fixed by fitting the diffraction pattern in Eq. (3) to the observed cross section. In the elastic scattering, a is derived by fitting to the first peak of the experimental cross section at $\theta_{\mathrm{c.m.}} > 0^\circ$ [16], while a for the inelastic scattering is determined from the fit to the second peak [7].

I fit the first diffraction peak of Eq. (3) at $\theta_{\mathrm{c.m.}} > 0^\circ$ to the first peak at $\theta_{\mathrm{c.m.}} \approx 5^\circ$, at which both of the differential cross sections show a prominent peak in Fig. 3, although the fit to the second peak is appropriate for determining the magnitude of the inelastic black-sphere radius [7]. This is because I mainly focus on a relative enhancement of 2_2^+ with respect to 2_1^+. The fit to the peak at $\theta_{\mathrm{c.m.}} \approx 5^\circ$ gives $a(2_1^+) = 4.95$ fm and $a(2_2^+) = 5.50$ fm, and hence, the enhancement of $\Delta a = a(2_2^+) - a(2_1^+)$ is $\Delta a \approx 0.6$ fm.

In order to analyze the relation of the differential cross sections (Fig. 3) and the enhanced diffraction radius more deeply, I have performed a partial wave analysis, in which the angle-integrated cross sections in Fig. 3 are decomposed into the individual components of the incident orbital spin L. The results of the decomposition are shown in Fig. 5. The dotted curve with open circles shows the partial wave distribution (L distribution) of the angle-integrated 2_1^+ cross section, while the L distribution of 2_2^+ is plotted by the solid curve with filled circles.

In the comparison of 2_1^+ with 2_2^+, one can clearly see the extended L distribution of 2_2^+ to the higher-L region. This extension of 2_2^+ in the L space (Fig. 5) is just opposite the shrinkage in the θ space, the differential cross section (Fig. 3). This is nothing but the uncertainty relation $L \cdot \theta \approx 1$, which can hold for the diffraction scattering. According to the classical relation $L = kb$, where k and b denote the incident momentum and the impact parameter, respectively, the extension of the L distribution in Fig. 5 clearly means that the production area of the 2_2^+ state is more extended than the area of 2_1^+ production. Since the difference between these two kinds of 2^+ final channels is merely the nuclear radius, the rapid decrease in θ space and extension of L space in the 2_2^+ must originate from the enhanced nuclear radius in the 2_2^+ state. Therefore, the enhancement by $\Delta a \approx 0.6$ fm can be attributed to an extended nuclear radius in the final 2_2^+ state.

I have extended the MCC calculation to the lower α incident energy $E_\alpha = 240$ MeV, where the diffraction pattern is not necessarily clear in the observed differential cross sections. In the lower energy region, unfortunately, there are no

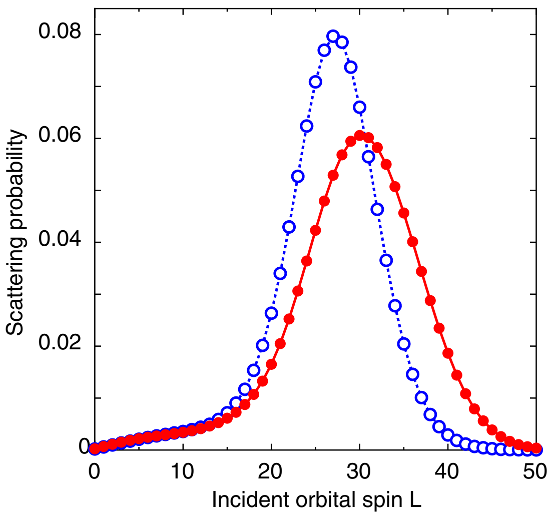

FIG. 5. Partial wave decomposition of angle-integrated cross sections calculated as a function of the incident orbital spin L (L distribution). The dotted curve with open circles shows the partial cross section of the 2_1^+ final channel; the solid curve with filled circles, that of the 2_2^+ final channel. The magnitudes of all the partial cross sections are normalized by the total cross section, which is the summation of the partial cross sections.

experimental data on the excited state at $E_x \approx 10$ MeV, which contains the 2_2^+ component. Therefore, the parameters of the absorptive potential of the 3α cluster states (0_2^+, 0_3^+, 2_2^+) are set to a common value, and the parameters are tuned so as to reproduce the cross section of 0_2^+ and 0_3^+ as much as possible. In this calculation, a differential cross section of 2_2^+ is predicted, and hence the difference of $d\sigma/d\Omega(2_2^+)$ and $d\sigma/d\Omega(2_1^+)$ can be evaluated.

In Fig. 6, a comparison of 2_1^+ (dotted curve) with 2_2^+ (solid curve) is shown. One can clearly observe the shrunken structure in the 2_2^+ channel over a wide angular range at $E_\alpha = 240$ MeV.

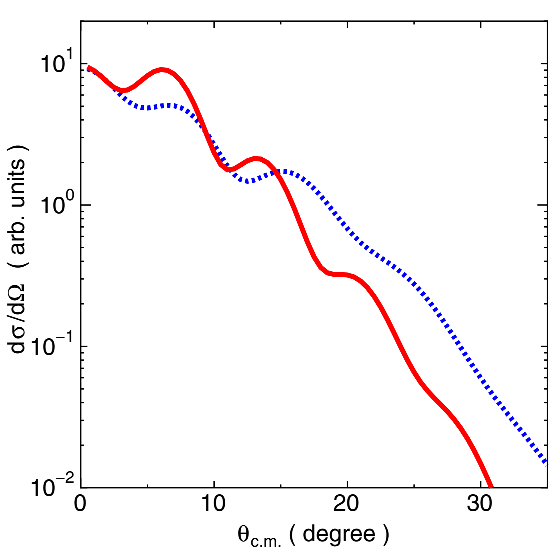

FIG. 6. Same as Fig. 3 except that the incident energy is $E_\alpha = 240$ MeV. The magnitudes of the cross sections are normalized to the first peak at $\theta_{\text{c.m.}} = 0^\circ$.

TABLE I. Difference in spatial size of the $2_{1,2}^+$ states. ΔR_{m} represents the difference in the nuclear radius $\Delta R_{\text{m}} = R_{\text{m}}(2_2^+) - R_{\text{m}}(2_1^+)$ with root mean squared radius R_{m}, while ΔR_{trd} represents the difference in the peak position of the transition density, that is, $\Delta R_{\text{trd}} = R_{\text{trd}}(2_2^+) - R_{\text{trd}}(2_1^+)$. Δa shows the difference in the diffraction radius, which is derived from the differential cross section at $E_\alpha = 386$ MeV. See text for details.

ΔR_{m}	ΔR_{trd}	Δa
1.6 fm	1.0 fm	0.6 fm

The diffraction radii, which are derived according to Blair's formula in Eq. (3), are $a(2_1^+) \approx 4.9$ fm and $a(2_2^+) \approx 5.9$ fm. In this analysis, the second peaks around $\theta_{\text{c.m.}} \approx 8^\circ$ are fitted to the peaks of the Bessel functions, although fitting is a little difficult in comparison to the high-energy scattering at $E_\alpha = 386$ MeV. Thus, in the lower-energy region, the difference in the diffraction radius, which reaches $\Delta a = 1$ fm, is more enhanced than the $\Delta a = 0.6$ fm obtained at $E_\alpha = 386$ MeV.

In Table I, the differences in the spatial size of the $2_{1,2}^+$ states are summarized. According to the structure calculation using the 3α resonating group method [4], the difference in the nuclear radius of the $2_{1,2}^+$ states is $\Delta R_{\text{m}} = R_{\text{m}}(2_2^+) - R_{\text{m}}(2_1^+) = 1.6$ fm (leftmost column), in which R_{m} is the root mean squared radius. The differential cross section for inelastic scattering is sensitive not to the final-state nuclear radius R_{m} but to the size of the transition density. In the size difference of the transition density (ΔR_{trd}), the large difference appearing in ΔR_{m} is reduced to be about 1 fm (middle column). Here the size difference in the transition density is defined by the difference in the peak position of the transition density with the multiplication of the squared radius, that is, $\Delta R_{\text{trd}} = R_{\text{trd}}(2_2^+) - R_{\text{trd}}(2_1^+)$, in which $r = R_{\text{trd}}$ gives the peak value for $r^2 \rho_{0_1^+ \to 2_{1,2}^+}(r)$. In the real inelastic scattering, the difference in the transition density is further reduced, and the difference in the diffraction radius, which represents the spatial size for the final-state production, is about 0.6 fm (rightmost column). This further reduction is due to the reaction dynamics, such as the incident energy, absorption effect, and channel coupling.

The enhancement of the diffraction radius of $\Delta a = 0.6$ fm is smaller than the original difference in the nuclear radius of $R_{\text{m}} = 1.6$ fm but one can still note a prominent enhancement of the diffraction radius, $\Delta a = 0.6$ fm, from the differential cross section. Furthermore, this diffraction radius is more enhanced in the lower-energy region. Thus, a more in-depth analysis of the reaction dynamics is needed to discuss the relation of the enhanced nuclear radius and inelastic scattering.

IV. SUMMARY

In summary, I have tried to obtain evidence of the enhanced nuclear radius of the Hoyle rotational state, 2_2^+, from the differential cross section of the $\alpha + {}^{12}\text{C}$ inelastic scattering. First, I have performed a microscopic coupled-channels (MCC) calculation and succeeded in reproducing the observed differential cross sections at $E_\alpha = 386$ MeV. In particular, the differential cross section of the excited state at $E_x \approx 10$ MeV has been nicely reproduced by taking the incoherent summation of the 2_2^+ and 0_3^+ channels. Second, the differential cross section of 2_2^+ with the 3α structure, which is derived from the incoherent fitting to the cross section of the $E_x \approx 10$ MeV state, is compared with the noncluster state, 2_1^+, which has a spatially compact structure.

In the comparison of the $2_{1,2}^+$ channels, one can clearly confirm that the inelastic differential cross section of the 2_2^+ channel is more shrunken than that of the 2_1^+ channel. This shrinkage is the first evidence of the extended nuclear radius of the final 2_2^+ state, which can be derived from the inelastic scattering of $\alpha + {}^{12}\mathrm{C}(0_1^+) \rightarrow \alpha + {}^{12}\mathrm{C}(2_2^+)$. The difference in the excitation energies of the $2_{1,2}^+$ states is checked but the effect of the excitation energy does not disturb the shrinkage structure in the 2_2^+ differential cross section. According to the prescription of the diffraction formula, the shrunken structure of the differential cross section can be converted into the spatial size. I have obtained an enhancement of about 0.6 fm in the size of the production area of the final 2_2^+ state. Furthermore, the enhancement of the diffraction radius is increased to about 1 fm at the lower incident energy $E_\alpha = 240$ MeV.

In order to examine the origin of the shrunken structure in the differential cross section, which is equivalent to the enhanced diffraction radius, in more depth, I have done a partial wave analysis of the cross section. The partial wave decomposition shows the extended distribution in the 2_2^+ channel, and this extended distribution means that the spatial size for 2_2^+ production is more extended than that for 2_1^+ production. Since the major difference in the inelastic scattering going to 2_1^+ and 2_2^+ is merely the spatial size of the final states, the shrunken structure in the angular distribution and the extended structure in the partial wave distribution can be attributed to the enhanced nuclear radius of the latter state, the 2_2^+ state. One can speculate that the enhanced nuclear radius of 2_2^+ is about 0.6 to 1 fm in comparison to the radius of 2_1^+.

I have shown that the enhanced radius of the 2_2^+ state can be probed via the differential cross section by comparison with the reference cross section of the 2_1^+ state. Comparison of the yrast 2_1^+ state and the Hoyle rotational 2_2^+ state is a new insight in the discussion of inelastic scattering of ^{12}C, which was absent from previous studies of the relation of the nuclear radius and the inelastic scattering to the Hoyle 0_2^+ state [6–10]. In the case of 0_2^+ production, there is no "inelastic 0^+ channel" that should be compared to the Hoyle 0_2^+ state. Therefore, the enhancement factor, which may be observed in the 0_2^+ channel, is difficult to catch in inelastic scattering.

The present analysis has demonstrated that the enhanced nuclear radius reaches 0.6–1.0 fm for the Hoyle rotational state in comparison to the radius of the 2_1^+ state. However, this enhancement in the 2_2^+ state can be regarded as the size enhancement from the ground 0_1^+ state because the nuclear radius of the 2_1^+ state is expected to be almost the same as the radius of the ground 0_1^+ state. About 1-fm enhancement in the nuclear radius of the 2_2^+ state is comparable to the extended radius in ^{11}Li [2], which largely deviates from the systematics of $\propto A^{1/3}$. ^{11}Li corresponds to the excited state from ^{11}B, in which the isospin degrees of freedom is excited. The excitation energy of ^{11}Li [BE(^{11}Li) − BE(^{11}B)] is about 34 MeV, while the excitation energy of $^{12}\mathrm{C}(2_2^+)$ is 10 MeV. Thus, the 1-fm enhancement in the nuclear radius in $^{12}\mathrm{C}(2_2^+)$ is an exotic phenomenon, which occurs at a much lower excitation energy than in the neutron-excess nucleus.

Furthermore, the identification of about 1-fm enhancement in the nuclear radius imposes a strong constraint on the recent *ab initio* calculation which seems to reproduce the excitation energy of the Hoyle 0_2^+ and 2_2^+ states [17]. In this structure calculation, the radius of the Hoyle rotational 2_2^+ state is almost the same as the radius of the ground state (2.4 fm) [17], which is much smaller than the prediction by the 3α cluster model (≈4.0 fm) [4,5]. The result of the *ab initio* calculation seems to be inconsistent with the enhanced radius that is obtained in the present analysis of scattering phenomena.

In previous studies, there was no information on the nuclear radius of the excited states that should be compared with the theoretical calculation. Therefore, speculation on the lower bound of the nuclear radius of the Hoyle rotational 2_2^+ state from the experimental observables will be quite important in future studies. Since the experimental information on the differential cross section of the 2_2^+ channel is still insufficient, measurement of the differential cross section of the excited state at $E_x \approx 10$ MeV and careful multipole decomposition analysis to separate the 2_2^+ component should be extended over a wide angle and incident energy region.

ACKNOWLEDGMENTS

The author is sincerely thankful to Professors H. Horiuchi, K. Iida, M. Itoh, K. Ogata, and T. Wada and Dr. K. Minomo for their valuable discussions and encouragement. He is deeply grateful to Professors T. Motobayashi and A. Kohama for careful reading of the manuscript and useful comments. This work was done in collaboration with Mr. M. Tomita, M. Iwasaki, R. Otani, and M. Nakao and supported by Grants-in-Aid for Scientific Research in Japan, KAKENHI (No. 26400284 and No. 17K05454).

APPENDIX

The parameters of the imaginary potentials are listed in Table II. With the introduction of the energy-dependent imaginary potential, the theoretical calculation nicely reproduces the observed angular distribution at the collision energies of $E_\alpha = 386$ MeV and 240 MeV.

TABLE II. Parameters of the absorptive Saxon-Woods potential at $E_\alpha = 386$ MeV. W_I, R_I, and a_I represent the depth, the radius, and the diffuseness, respectively.

Channel	W_I (MeV)	R_I (fm)	a_I (fm)
0_1^+	20.0	3.40	0.60
0_2^+	30.0	5.00	0.80
0_3^+	60.0	4.50	0.70
2_1^+	28.0	4.00	0.60
2_2^+	20.0	6.50	0.70
3_1^-	30.0	3.50	0.80

[1] P. Ring and P. Schuck, *Nuclear Many-Body Problem*, 1st ed. (Springer-Verlag, Berlin, 2004).

[2] I. Tanihata, H. Savajols, and R. Kanungo, Prog. Part. Nucl. Phys. **68**, 215 (2013).

[3] K. Ikeda *et al.*, Prog. Theor. Phys. **68**, 1 (1980).

[4] Y. Fukushima and M. Kamimura, J. Phys. Soc. Jpn. **44**, 225 (1978); M. Kamimura, Nucl. Phys. A **351**, 456 (1981).

[5] Y. Funaki, A. Thosaki, H. Horiuchi, P. Schuck, and G. Reöpke, Eur. Phys. J. A **24**, 321 (2005), and references therein.

[6] A. N. Danilov, T. L. Belyaeva, A. S. Demyanova, S. A. Ganchalov, and A. A. Ogloblin, Phys. Rev. C **80**, 054603 (2009).

[7] K. Iida, S. Koide, A. Kohama, and K. Oyamatsu, Mod. Phys. Lett. A **27**, 1250020 (2012).

[8] S. Ohkubo and Y. Hirabayashi, Phys. Rev. C **70**, 041602(R) (2004).

[9] M. Takashina and Y. Sakuragi, Phys. Rev. C **74**, 054606 (2006).

[10] M. Takashina, Phys. Rev. C **78**, 014602 (2008).

[11] M. Itoh *et al.*, Phys. Rev. C **84**, 054308 (2011).

[12] M. Ito, Y. Hirabayashi, and Y. Sakuragi, Phys. Rev. C **66**, 034307 (2002), and references therein.

[13] A. M. Kobos, B. A. Brown, P. E. Hodgson, G. R. Satchler, and A. Budzanowski, Nucl. Phys. A **384**, 65 (1982).

[14] M. Tomita, M. Iwasaki, R. Otani, and M. Ito, Phys. Rev. C **89**, 034619 (2014).

[15] J. S. Blair, Phys. Rev. **115**, 928 (1959).

[16] A. Kohama, K. Iida, and K. Oyamatsu, J. Phys. Soc. Jpn. **85**, 094201 (2016), and references therein.

[17] E. Epelbaum, H. Krebs, T. A. Lähde, D. Lee, and Ulf-G. Meißner, Phys. Rev. Lett. **109**, 252501 (2012), and references therein.